

Self-Induced Valley Bosonic Stimulation of Exciton Polaritons in a Monolayer Semiconductor

Pasquale Cilibrizzi, Xiaoze Liu, Peiyao Zhang, Chenzhe Wang[✉], Quanwei Li[✉], Sui Yang[✉], and Xiang Zhang
NSF Nanoscale Science and Engineering Center, University of California, Berkeley, California 94720, USA



(Received 24 July 2021; accepted 18 November 2022; published 20 January 2023)

The newly discovered valley degree of freedom in atomically thin two-dimensional transition metal dichalcogenides offers a promising platform to explore rich nonlinear physics, such as spinor Bose-Einstein condensate and novel valleytronics applications. However, the critical nonlinear effect, such as valley polariton bosonic stimulation, has long remained an unresolved challenge due to the generation of limited polariton ground state densities necessary to induce the stimulated scattering of polaritons in specific valleys. Here, we report the self-induced valley bosonic stimulation of exciton polaritons via spin-valley locking in a WS_2 monolayer microcavity. This is achieved by the resonant injection of valley polaritons at specific energy and wave vector, which allows spin-polarized polaritons to efficiently populate their ground state and induce a valley-dependent bosonic stimulation. As a result, we observe the nonlinear self-amplification of polariton emission from the valley-dependent ground state. Our finding paves the way for the investigation of spin ordering and phase transitions in transition metal dichalcogenides polariton Bose-Einstein condensate, offering a promising route for the realization of polariton spin lattices in moiré polariton systems and spin lasers.

DOI: [10.1103/PhysRevLett.130.036902](https://doi.org/10.1103/PhysRevLett.130.036902)

The optical properties of a semiconductor are intrinsically related to its electronic band structure. The broken inversion symmetry in recently emerging two-dimensional transition metal dichalcogenides (TMDs) leads to two energy degenerate valleys at two corners of the first Brillouin zone, referred to as K/K' valleys [1,2]. Strong spin-orbit coupling locks the valley degree of freedom to the electron and hole spins (i.e., spin-valley locking), resulting in specific optical selection rules of excitons [3]. Specifically, excitons in K/K' valleys can be selectively addressed using $\sigma + / \sigma -$ circularly polarized optical excitations. These intriguing properties and the possibility to control valley degree of freedom open new ways to explore spinor or valleytronic physics and novel valleytronics applications [4].

TMD exciton polaritons (hereafter polaritons), resulting from the strong coupling of cavity photons with TMD excitons [5], are composite bosonic quasiparticles, which can also be optically initialized in specific valleys [6–10]. Recently, TMD polaritons have emerged as promising candidates for studying fundamental polaritonic physics and nonlinearities [11–13]. Different polariton nonlinear behaviors have been explored so far, leading to the observation of polariton condensation [11,12] and moiré nonlinearities [13]. Both these observations result from polariton-polariton interactions inherited by the underlying TMD excitons' Coulomb interactions. Furthermore, polariton interactions are spin dependent [14]. The spin interactions enrich the physics of polariton condensates, giving rise to many fascinating topological effects in quantum fluids [15]. In this regard, the valley degree of freedom

represents an additional experimental knob to control polariton spin interactions in the nonlinear regime. It offers the possibility to engineer polariton spin interactions in microcavities and control stochastic spin phenomena in spinor Bose-Einstein condensate (BEC) [16], allowing, for example, the realization of different spin configurations when the polarization of the polariton condensates is pinned to a specific crystallographic axis of the microcavity [17,18]. The possibility to control ferromagnetic spin interactions in polariton condensates provides new opportunities to experimentally investigate the complex interplays between magnetic order and superfluidity in polariton BECs [19] and explore spin order and phase transitions in moiré polariton systems [13]. However, so far, the valley degree of freedom has been mainly studied in the linear regime. In such a regime, the most fascinating polaritonic physics, such as BEC and superfluidity [14], is precluded.

A critical step to advance TMD polaritons, as a practical platform to manipulate spin interactions in polariton BEC [20] and superfluid, is the realization of the valley bosonic stimulation, that is the nonlinear amplification of polaritons in specific valleys. The valley bosonic stimulation, however, has remained a major challenge, due to the significant difficulties in generating the polariton ground-state densities necessary to induce the stimulated scattering of polaritons in desired valleys. Nonresonant experiments have been studied in which the generation of polaritons is mediated by the population of an exciton reservoir. Yet they usually suffer from the reduced photoluminescence (PL) emission, due to exciton-exciton

annihilation processes [21,22] and additional valley depolarization effects, induced by exciton-exciton Coulomb exchange interactions [23,24].

Here, we demonstrate the self-induced valley bosonic stimulation in a WS_2 monolayer microcavity. To generate the polariton densities necessary to induce the self-stimulated scattering of polaritons in desired valleys, we resonantly inject polaritons at specific energy and wave vector (k) [25] and with specific spin orientation. Since polaritons are resonantly injected in the microcavity, we do not create an exciton reservoir, thus limiting the density-dependent excitonic effects responsible for the reduction of valley polarization in TMD monolayers [23]. The observed nonlinear behaviour emerges directly from polariton-polariton interactions, and it is not mediated by other type of interactions (e.g., interactions of polaritons with the exciton reservoir and/or the injected photocarriers), which usually dominate the polariton dynamics and nonlinearity in non-resonant excitation experiments [26]. We observe the nonlinear increase of the polariton emission co-polarized with the pump, a key signature of the valley bosonic stimulation. This process is facilitated by the spin-valley locking mechanism inherited by TMD polaritons from their exciton components, allowing polaritons to efficiently retain their valley polarization during their energy and momentum relaxation. Our findings show that polaritons can undergo a self-induced valley-dependent bosonic stimulation, which is the first step toward the realization of spinor polariton BECs in atomically thin TMD monolayers, allowing control and manipulation of spin interactions in polariton lattices and moiré polariton systems for quantum simulations.

The valley bosonic stimulation corresponds to the amplification of polariton emission in specific valleys. The underlying conditions to observe this effect are (i) the possibility to selectively populate polaritons in specific valley and (ii) the preservation of the valley population as polaritons scatter towards the ground state. The spin-valley locking behavior inherited from TMD excitons [Fig. 1(a)], persists onto the hybrid polariton state, thus ensuring the generation of a ground state polariton population, co-polarized with the pump [condition (i), σ^- in Fig. 1(b)]. Since the energy and momentum relaxation of polaritons are spin dependent [27], spin-down (-up) ground state polaritons stimulate the scattering of other high-energy spin-down (-up) polaritons [condition (ii), Fig. 1(b)]. Thus, upon increasing the polariton density, the valley bosonic stimulated scattering leads to the nonlinear amplification of the PL intensity and a high degree of valley polarization in momentum space.

The microcavity sample consists of a single monolayer WS_2 embedded between two distributed Bragg reflectors (DBRs), grown on top of a silicon substrate, as schematically shown in Fig. 2(a). We report the fabrication details and the optical characterization of the microcavity in the

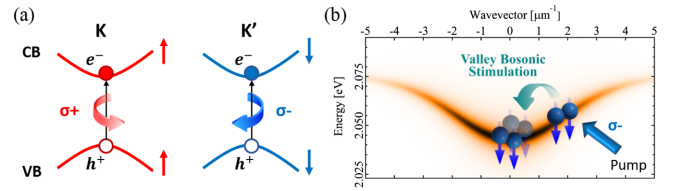


FIG. 1. (a) Schematic of the spin-valley locking mechanism. Two degenerate valleys form in the WS_2 monolayer due to the absence of crystal inversion symmetry. Spin-orbit coupling locks the valley index (K, K') to the electron (e^-) and hole (h^+) spins (up, down arrows), resulting in specific exciton optical selection rules. Excitons with opposite spins ($+1/-1$) can be created in different valleys in momentum space (K/K'), utilizing circular polarized optical excitations ($\sigma+/\sigma-$). (b) Schematic of the polariton valley bosonic stimulation induced by the resonant excitation scheme (blue arrow, “Pump”). Polaritons (blue spheres) resonantly injected in the lower polariton branch, with a spin set by the polarization of the pump ($\sigma-$), scatter towards the $k \sim 0$ energy state. The presence of $\sigma-$ polaritons at $k \sim 0$ stimulates the scattering of other polaritons with parallel spins, resulting in the self-amplification of polariton emission from the valley-dependent ground state.

Supplemental Material [28]. In the experiments, the sample is held in a cold finger cryostat at 80 K temperature. To excite the microcavity, we use a visible laser with a central wavelength of 603.2 nm (~ 2.056 eV). The excitation laser (see Supplemental Material [28] for details) is spectrally filtered, to obtain pump pulses of 3 meV FWHM, as shown in Fig. 2(b) (red profile). The excitation beam is circularly polarized (σ_+ or σ_-) and focused to a 1.7 μm FWHM spot diameter using a 0.60 numerical aperture microscope objective. PL from the lower-polariton branch is collected in reflection geometry through the excitation microscope objective (with $\pm 37^\circ$ collection angle). The emission from the lower-polariton branch is spectrally filtered, allowing the detection of polaritons populating the bottom of the lower-polariton dispersion at energy ≤ 2.047 eV, while suppressing the excitation laser [Fig. 2(b)]. The PL is then analyzed by a polarimeter, composed of $\lambda/4$ and $\lambda/2$ plates plus a linear polarizer, and projected on the entrance slit of a spectrometer (see Supplemental Material [28] for details). To excite the microcavity with a specific angle, the excitation beam enters the focusing objective off center. We select the specific excitation angle by imaging simultaneously the pump laser and the PL emission, as shown in the Supplemental Material (S2) [28]. The angle and energy of excitation used in the experiments have been estimated in the Supplemental Material (S3) [28], by considering the scattering relaxation mechanism of polaritons with higher energy, under resonant excitation [14].

Experimentally, the bosonic stimulation regime can be probed by driving the system resonantly with the excitation laser and performing energy and wave vector resolved spectroscopy [Fig. 2(b)]. Specifically, we excite the sample at $E_p = 2.056$ eV and $\theta_p = 11^\circ$ angle. These excitation

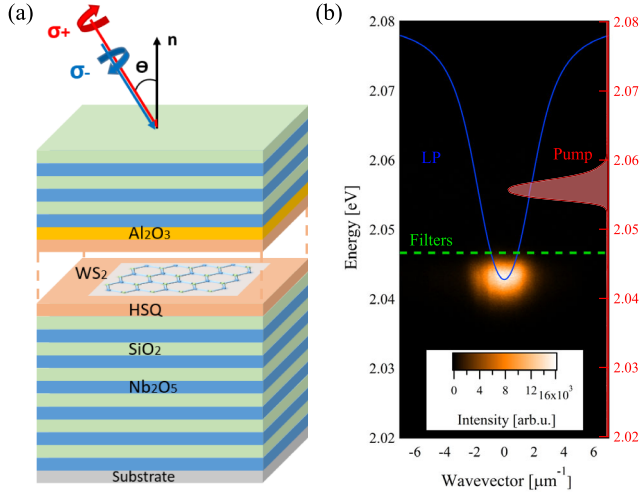


FIG. 2. (a) Schematic of the microcavity sample, composed of two ($\text{Nb}_2\text{O}_5/\text{SiO}_2$) DBRs and a WS_2 monolayer sandwiched between two protective (HSQ and Al_2O_3) layers (see Supplemental Material [28] for details). The microcavity is excited with a σ_+ (σ_-) polarized beam set at an angle of incidence (Θ), relative to the microcavity’s normal axis (n). (b) Experimental energy-wave vector resolved emission intensity measured under resonant σ_+ -excitation, σ_+ -detection ($137 \mu\text{J}/\text{cm}^2$ pump fluence). The red trace (“Pump”) corresponds to the pump laser intensity profile used in the experiments. To filter out the excitation laser, we spectrally filter the emission from the microcavity sample, as indicated by the green dotted line and detect the PL polariton emission from the ground state of the lower-polariton dispersion.

parameters allow us to resonantly generate polaritons at $k_p = 1.9 \mu\text{m}^{-1}$ close to the inflection point of the lower-polariton dispersion. To filter out the excitation laser, we spectrally filter the emission from the microcavity, as indicated by the green dotted line in Fig. 2(b) and detect the polariton emission from the lowest energy state of the polariton dispersion. Polaritons injected at E_p and k_p relax down to their ground state, populate the bottom of the lower-polariton dispersion at $k \sim 0$ and leak out through the top DBR [29]. By repeating the reciprocal space spectroscopic imaging under nonresonant optical excitation (see Supplemental Material [28], S4), we collect the lower-polariton dispersion (Fig. S4b) and confirm that the PL emission we detect in our resonant experiments [Fig. 2(b)] corresponds to polaritons that accumulate in the lowest energy state (at $k \sim 0$) of the dispersion.

To demonstrate the valley bosonic stimulation of polaritons into the lowest-energy polariton states at $k \sim 0$, circularly polarized power dependence measurements are performed with selected excitation of σ_+/σ_- polarized polaritons in both K/K' valleys. The dependences of the intensity (i.e., peak intensity), linewidth (i.e., FWHM), and the central energy (i.e., peak energy) of the polariton emission at different excitation densities were studied by fitting the PL spectra with a single Gaussian function. The PL spectra are extracted as intensity profiles along the

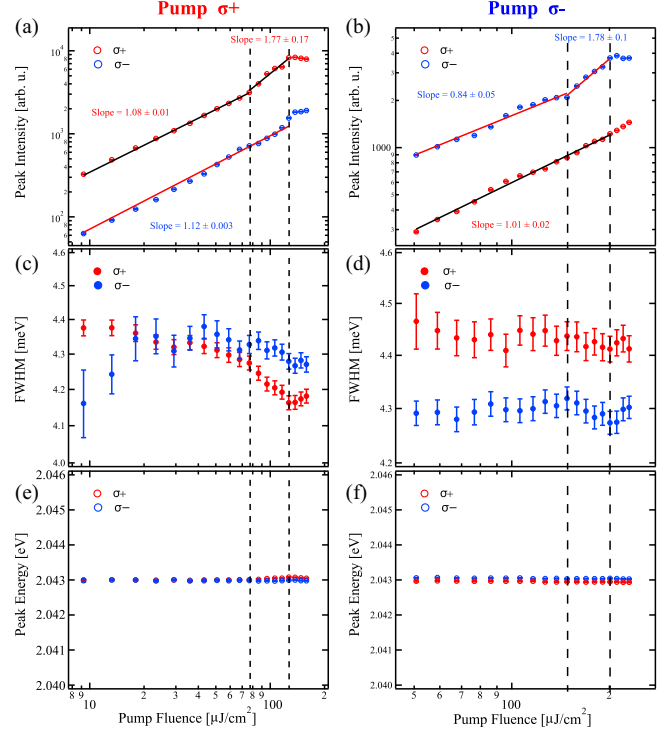


FIG. 3. (a) The nonlinear increase of the polariton PL intensity co-polarized with the σ_+ excitation pump (red circles), showing K -valley polaritons undergo valley bosonic stimulation. (b) The nonlinear increase of the polariton PL intensity co-polarized with the σ_- excitation pump, confirming the valley bosonic stimulation also in the K' valley (blue circles). In both cases, the cross-polarized PL intensities, σ_- in (a) and σ_+ in (b), exhibit only a linear increase with increasing fluence, as it corresponds to the intervalley scattering of polaritons. (c)–(f) With increasing excitation density, the linewidths of polaritons co-polarized with the σ_+ (c) and σ_- (d) excitation pump narrow, while the peak energy does not change (e),(f). All the data are plotted on a log-log scale. The data in (a)–(b) are fitted with $y(x) = kx^n$, where n represents the slope of the lines used in the fittings. Error bars are extracted from the fits. For (a),(b),(e),(f) the error bars are too small to be visible. The vertical dotted lines highlight the nonlinear emission regime.

y axis (i.e., energy) at $|k| < 2.6 \mu\text{m}^{-1}$ of the k -space emission data [e.g., Fig. 2(b)] at different excitation densities. By increasing the circularly polarized (σ_+) excitation fluence, we increase the polariton density and observe a nonlinear increase of the intensity [Fig. 3(a), red circles], together with a linewidth narrowing [Fig. 3(c), red circles], from 4.27 ± 0.02 (below threshold) to 4.16 ± 0.02 meV (above threshold), of the co-polarized polaritons emission at the nonlinear photoluminescence threshold. These features are hallmarks of lasing, condensation, and buildup of temporal coherence. We do not observe, however, any obvious blueshift of the peak position with the increasing excitation density [Fig. 3(e)], as in the case of polariton condensates [20].

We also confirm the valley nonlinear behavior in the K' valley, by exciting the microcavity with the opposite

circular polarization (σ_-) and detecting the co-polarized polaritons. Also in this case, the intensity of the co-polarized polariton emission [Fig. 3(b), blue circles] increases nonlinearly with the same slope as in the K valley, the linewidth drops [from 4.32 ± 0.02 to 4.27 ± 0.02 meV in Fig. 3(d)], while the peak position does not change in energy with the increasing excitation density [Fig. 3(f)]. The nonlinear increase of the polariton emission from the lowest energy states is a clear signature of the bosonic final-state stimulation, which is a statistical property of bosons and the driving mechanism behind matter-wave amplification of both atomic [30] and polariton [20] BEC. The bosonic stimulation occurs under less stringent conditions than BEC. The scattering rate of bosons into a certain quantum state is proportional to the number of bosons occupying that state. In particular, the presence of N bosons in the final state enhances the scattering rate of other bosons (by a factor $1 + N$), thus effectively accelerating the energy relaxation process and stimulating the scattering of other identical bosons in the same state [29]. Therefore, with increasing polariton density, the co-polarized polariton relaxation rate increases, eventually overcoming the threshold for bosonic stimulation. Specifically, this occurs when the relaxation of polaritons towards the ground state overcome its radiative decay, resulting in a superlinear increase of the polariton density at the bottom of the lower-polariton dispersion in both K/K' valleys. Since excitons in TMD monolayers have identical valley-dependent optical response [1], the different thresholds that we observe are due to the generation of different polariton densities in the two valleys, at fixed σ_+/σ_- excitation power. The latter may be due to the presence of strain on the monolayer, affecting the TMD selection rules [31], and to an unequal excitation of the transverse-electric–transverse-magnetic (TE-TM) polariton modes. At fixed excitation angle and energy, the polariton TE-TM polarization splitting [14], inherited from the cavity [32] and the TMD excitons [33], can result in different σ_+/σ_- polariton densities, for an unequal excitation of the TE/TM polariton modes inside the cavity. Since the threshold is ultimately determined by the polariton density in each valley, the valley less populated requires a higher excitation density to reach the bosonic stimulation threshold. However, despite this difference, the nonlinear emission and the linewidth-narrowing that we observe in both valleys, confirm the valley nature of the bosonic stimulation. This is further corroborated by the observation of a self-amplification in both valleys (see Supplemental Material [28]), reaching a maximum of 1.7, comparable with pump-probe amplifications, observed in similar TMD microcavities, with enhanced polaron-polaritons interactions [34].

Conversely, the cross-circular polarized PL intensities, corresponding to polaritons scattering in the opposite valley with respect to the one where they were initially generated (i.e., intervalley scattering), show only a linear

increase with increasing fluence and a nearly constant (i.e., within the error bars) linewidth. This confirms that, by resonantly injecting polaritons in the lower-polariton dispersion at specific energy and wave vector, we can generate the polariton density necessary to induce the bosonic stimulation of polaritons in the same valley, thus facilitating the intravalley scattering of polaritons to overcome the intervalley scattering, typical of WS_2 excitons [35]. In our experiments, no injection of an initial population of polaritons at $k \sim 0$ is required to stimulate the scattering of polaritons in the lowest energy state as, for example, in optical parametric amplification experiments [25]. Similarly, we do not measure any polariton emission at energy and wave vectors above the excitation laser (i.e., “idler” state [25]). We observe a self-induced valley bosonic stimulation in the polariton ground state, confirming that our resonant excitation scheme allows, in each valley, an efficient relaxation of polaritons toward the bottom of their dispersion and the generation of polaritons density sufficient to overcome the stimulation threshold. The bosonic stimulation occurs at pump fluences lower than nonlinear scattering processes in other materials, such as, for example, BBO crystals [36], confirming the high interacting nature of TMD polaritons.

Finally, the spin-valley locking mechanism is uniquely probed by the generation of valley polaritons and the conservation of their spin in each valley (Fig. 4). To investigate the spin conservation of polaritons associated with their valley polarization, we measured the circular degree of polarization (CDP) from the polarization-resolved k -space spectroscopy images acquired during the power dependence measurements. As expected from the optical selection rules, a σ_+ (σ_-) circularly polarized excitation beam, will generate co-polarized polaritons in K (K') valley in momentum space (Fig. 4). In other words, resonantly injected polaritons in K (K') valley highly retain the σ_+ (σ_-) circular polarization of the pump during

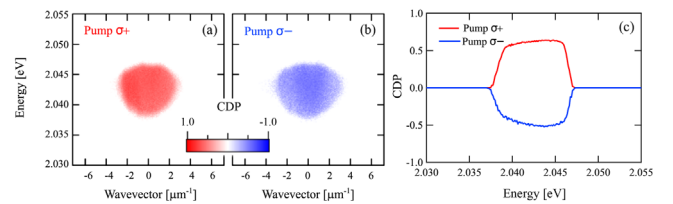


FIG. 4. The degree of circular polarization of the (a) K and (b) K' valley ground state polariton emission in momentum space. σ_+ (σ_-) polaritons, co-polarized with the pump, scatter toward the bottom of the lower-polariton dispersion and uniformly populate the $k \sim 0$ energy state in the K (K') valley. The σ_+ (σ_-) circular polarization of the pump is largely preserved by K (K') valley polaritons, resulting in a positive (negative) sign of the CDP in each valley. Here, $\text{CDP} = (I_{\sigma_+} - I_{\sigma_-}) / (I_{\sigma_+} + I_{\sigma_-})$, with I_{σ_+} and I_{σ_-} being the measured intensities of the two circular polarization components. (c) Vertical profiles extracted at $|k| < 1 \mu\text{m}^{-1}$ from (a) and (b).

their energy and momentum relaxation. The nonunitary circular degree of polarization that we observe is due to additional depolarization mechanisms. Many experimental studies [24,35] have shown that the spin relaxation dynamics in TMDs is dominated by the presence of at least two main depolarization mechanisms: (i) the Maialle-Silve-Sham mechanism [37], which is induced by the longitudinal-transverse splitting of the exciton energy and, ultimately, by the long-range Coulomb exchange interaction between the electrons and holes composing the excitons [38,39]; (ii) the intervalley scattering, due to both the long- and short-range exchange interactions [39] and the scattering by acoustic phonons [40,41]. In addition, in tungsten-based materials, the depolarization processes are more pronounced than in other TMD materials, due to the presence of an extra depolarization mechanism, such as the Γ -valley assisted intervalley scattering [35]. Thus, a maximum valley polarization of $\sim 35\%$ has been reported in WS_2 monolayers at both cryogenic (≤ 90 K) [42] and room temperature [42,43]. The combination of the spin-valley locking mechanism of TMD materials and the faster energy relaxation dynamics induced by the valley bosonic stimulation, allows us to observe a maximum degree of valley polarization of 64% for the K valley in WS_2 monolayers, which usually displays a low degree of valley polarization as a bare monolayer [42,43].

In summary, the following three experimental observations represent a clear indication of the valley bosonic stimulation: (i) the observation of the quadratic nonlinearity in K and K' valley, (ii) the lack of nonlinearity in the opposite valley (respect to where polaritons are generated), (iii) the narrowing of the FWHM in both valleys. The first two effects can only be realized if the rate at which polariton scatters toward $k \sim 0$ state is proportional to its occupation number in each valley. The narrowing of the FWHM, indicating an increase of the coherence time, can only occur for a macroscopically occupied valley polariton mode. Taken together these observations indicate that our resonant excitation scheme allows us to overcome TMD depolarization effects [35,38–41], a major obstacle for valley polariton nonlinear studies, suggesting a possible route for realizing strongly spin-polarized polariton condensates and polariton spin lattice for quantum simulations [44] above cryogenic temperature.

In conclusion, we have demonstrated the self-induced valley bosonic stimulation of exciton-polaritons in a monolayer TMD semiconductor. By coherently injecting polaritons at specific energy and wave vector of the lower-polariton dispersion, we overcome the challenges of generating valley polariton densities necessary to explore valley nonlinear processes in TMD microcavities. More importantly, the valley polariton stimulated scattering leads to the unique spin-valley locking nonlinear amplification of the polariton emission, despite the prominent valley depolarization processes typical of TMD materials.

The valley-dependent bosonic stimulation offers a new experimental knob for harnessing spin-dependent polariton interactions in the nonlinear regime, paving the way for the realization of spin-polarized polariton BEC in atomically thin TMD monolayers, polariton spin lattices in TMD monolayers and moiré heterostructures, as well as low-threshold spin-polarized lasers.

This work was supported by the Gordon and Betty Moore Foundation (Grant No. 5722) and the Ernest S. Kuh Endowed Chair Professorship.

-
- [1] X. Xu, W. Yao, D. Xiao, and T.F. Heinz, Spin and pseudospins in layered transition metal dichalcogenides, *Nat. Phys.* **10**, 343 (2014).
 - [2] K. Mak and J. Shan, Photonics and optoelectronics of 2D semiconductor transition metal dichalcogenides, *Nat. Photonics* **10**, 216 (2016).
 - [3] K. Mak, K. He, J. Shan, and T.F. Heinz, Control of valley polarization in monolayer MoS₂ by optical helicity, *Nat. Nanotechnol.* **7**, 494 (2012).
 - [4] J. Schaibley, H. Yu, G. Clark, P. Rivera, J. S. Ross, K. L. Seyler, W. Yao, and X. Xu, Valleytronics in 2D materials, *Nat. Rev. Mater.* **1**, 16055 (2016).
 - [5] C. Schneider, M. M. Glazov, T. Korn, S. Höfling, and B. Urbaszek, Two-dimensional semiconductors in the regime of strong light-matter coupling, *Nat. Commun.* **9**, 2695 (2018).
 - [6] Z. Sun, J. Gu, A. Ghazaryan *et al.*, Optical control of room-temperature valley polaritons, *Nat. Photonics* **11**, 491 (2017).
 - [7] Y.J. Chen, J. Cain, T. Stanev, V. P. Dravid, and N. P. Stern, Valley-polarized exciton-polaritons in a monolayer semiconductor, *Nat. Photonics* **11**, 431 (2017).
 - [8] S. Dufferwiel, T. Lyons, D. Solnyshkov *et al.*, Valley-addressable polaritons in atomically thin semiconductors, *Nat. Photonics* **11**, 497 (2017).
 - [9] G. Grosso, Valley polaritons, *Nat. Photonics* **11**, 455 (2017).
 - [10] M. Król, K. Lekenta, R. Mirek *et al.*, Valley polarization of exciton-polaritons in monolayer WSe₂ in a tunable microcavity, *Nanoscale* **11**, 9574 (2019).
 - [11] Jiaxin Zhao, Rui Su, Antonio Fieramosca, Weijie Zhao, Wei Du, Xue Liu, Carole Diederichs, Daniele Sanvitto, Timothy C. H. Liew, and Qihua Xiong, Ultralow threshold polariton condensate in a monolayer semiconductor microcavity at room temperature, *Nano Lett.* **21**, 3331 (2021).
 - [12] C. Anton-Solanas, M. Waldherr, M. Klaas *et al.*, Bosonic condensation of exciton-polaritons in an atomically thin crystal, *Nat. Mater.* **20**, 1233 (2021).
 - [13] L. Zhang, F. Wu, S. Hou, Z. Zhang, Y.-H. Chou, K. Watanabe, T. Taniguchi, S.R. Forrest, and H. Deng, Van der Waals heterostructure polaritons with moiré-induced nonlinearity, *Nature (London)* **591**, 61 (2021).
 - [14] A. Kavokin, J. J. Baumberg *et al.*, *Microcavities* (Oxford University Press, New York, 2011).
 - [15] H. Yang and N. Y. Kim, Microcavity exciton-polariton quantum spin fluids, *Adv. Quantum Technol.* **5**, 2100137 (2022).

- [16] H. Ohadi, A. Dreismann, Y. G. Rubo, F. Pinsker, Y. delValle-InclanRedondo, S. I. Tsintzos, Z. Hatzopoulos, P. G. Savvidis, and J. J. Baumberg, Spontaneous Spin Bifurcations and Ferromagnetic Phase Transitions in a Spinor Exciton-Polariton Condensate, *Phys. Rev. X* **5**, 031002 (2015).
- [17] Ł. Kłopotowski, M. D. Martín, A. Amo, L. Viña, I. A. Shelykh, M. M. Glazov, G. Malpuech, A. V. Kavokin, and R. André, Optical anisotropy and pinning of the linear polarization of light in semiconductor microcavities, *Solid State Commun.* **139**, 511 (2006).
- [18] R. Balili, V. Hartwell, D. Snoke, L. Pfeiffer, and K. West, Bose-Einstein condensation of microcavity polaritons in a trap, *Science* **316**, 1007 (2007).
- [19] Dan M. Stamper-Kurn and Masahito Ueda, Spinor Bose gases: Symmetries, magnetism, and quantum dynamics, *Rev. Mod. Phys.* **85**, 1191 (2013).
- [20] J. Kasprzak, M. Richard, S. Kundermann *et al.*, Bose-Einstein condensation of exciton-polariton, *Nature (London)* **443**, 409 (2006).
- [21] Y. Yu, Y. Yu, C. Xu, A. Barrette, K. Gundogdu, and L. Cao, Fundamental limits of exciton-exciton annihilation for light emission in transition metal dichalcogenide monolayers, *Phys. Rev. B* **93**, 201111(R) (2016).
- [22] Y. Lee, G. Ghimire, S. Roy, Y. Kim, C. Seo, A. K. Sood, J. I. Jang, and J. Kim, Impeding exciton-exciton annihilation in monolayer WS₂ by laser irradiation, *ACS Photonics* **5**, 2904 (2018).
- [23] F. Mahmood, Z. Alpichshev, Y.-H. Lee, J. Kong, and N. Gedik, Observation of exciton-exciton interaction mediated valley depolarization in monolayer MoSe₂, *Nano Lett.* **18**, 223 (2018).
- [24] D. Lagarde, L. Bouet, X. Marie, C. R. Zhu, B. L. Liu, T. Amand, P. H. Tan, and B. Urbaszek, Carrier and Polarization Dynamics in Monolayer MoS₂, *Phys. Rev. Lett.* **112**, 047401 (2014).
- [25] P. G. Savvidis, J. J. Baumberg, R. M. Stevenson, M. S. Skolnick, D. M. Whittaker, and J. S. Roberts, Angle-Resonant Stimulated Polariton Amplifier, *Phys. Rev. Lett.* **84**, 1547 (2000).
- [26] M. Pieczarka *et al.*, Effect of optically induced potential on the energy of trapped exciton polaritons below the condensation threshold, *Phys. Rev. B* **100**, 085301 (2019).
- [27] I. A. Shelykh, A. V. Kavokin, and G. Malpuech, Spin dynamics of exciton-polaritons in microcavities, *Phys. Status Solidi B* **242**, 2271 (2005).
- [28] See Supplemental Material at <http://link.aps.org/supplemental/10.1103/PhysRevLett.130.036902> for detailed descriptions of: (S1) the fabrication and optical characterization of the microcavity sample, (S2) the experimental verification of the excitation angle used in the experiments, (S3) the estimation of the excitation parameters, (S4) the comparison of the polariton dispersion obtained under resonant and non-resonant excitation, (S5) additional details on the polariton linewidth in the nonlinear regime, (S6) the circularly polarized power dependence measurements performed at a different excitation energy, (S7) the estimation of the maximum amplification of the polariton emission in the two valleys, (S8) the experimental setup.
- [29] H. Deng, H. Haug, and Y. Yamamoto, Exciton-polariton Bose-Einstein condensation, *Rev. Mod. Phys.* **82**, 1489 (2010).
- [30] H.-J. Miesner, D. M. Stamper-Kurn, M. R. Andrews, D. S. Durfee, S. Inouye, and W. Ketterle, Bosonic stimulation in the formation of a Bose-Einstein condensate, *Science* **279**, 1005 (1998).
- [31] M. M. Glazov, Florian Dirnberger, Vinod M. Menon, T. Taniguchi, K. Watanabe, D. Bougeard, J. D. Ziegler, and A. Chernikov, Exciton fine structure splitting and linearly polarized emission in strained transition-metal dichalcogenide monolayers, *Phys. Rev. B* **106**, 125303 (2022).
- [32] Giovanna Panzarini, Lucio Claudio Andreani, A. Armitage, D. Baxter, M. S. Skolnick, V. N. Astratov, J. S. Roberts, A. V. Kavokin, M. R. Vladimirova, and M. A. Kaliteevski, Exciton-light coupling in single and coupled semiconductor microcavities: Polariton dispersion and polarization splitting, *Phys. Rev. B* **59**, 5082 (1999).
- [33] M. M. Glazov, T. Amand, X. Marie, D. Lagarde, L. Bouet, and B. Urbaszek, Exciton fine structure and spin decoherence in monolayers of transition metal dichalcogenides, *Phys. Rev. B* **89**, 201302(R) (2014).
- [34] Li Bing Tan, Ovidiu Cotlet, Andrea Bergschneider, R. Schmidt, P. Back, Y. Shimazaki, M. Kroner, and A. Imamoglu, Interacting Polaron-Polaritons, *Phys. Rev. X* **10**, 021011 (2020).
- [35] H. Su, A. Deng, Z. Zhen, and J.-F. Dai, Γ -valley assisted intervalley scattering in monolayer and bilayer WS₂ revealed by time-resolved Kerr rotation spectroscopy, *Phys. Rev. B* **97**, 115426 (2018).
- [36] C. Manzoni and G. Cerullo, Design criteria for ultrafast optical parametric amplifiers, *J. Opt.* **18**, 103501 (2016).
- [37] M. Z. Maialle, E. A. de Andrada e Silva, and L. J. Sham, Exciton spin dynamics in quantum wells, *Phys. Rev. B* **47**, 15776 (1993).
- [38] M. M. Glazov, T. Amand, X. Marie, D. Lagarde, L. Bouet, and B. Urbaszek, Exciton fine structure and spin decoherence in monolayers of transition metal dichalcogenides, *Phys. Rev. B* **89**, 201302(R) (2014).
- [39] T. Yu and M. W. Wu, Valley depolarization due to intervalley and intravalley electron-hole exchange interactions in monolayer MoS₂, *Phys. Rev. B* **89**, 205303 (2014).
- [40] H.-Z. Lu, W. Yao, D. Xiao, and S.-Q. Shen, Intervalley Scattering and Localization Behaviors of Spin-Valley Coupled Dirac Fermions, *Phys. Rev. Lett.* **110**, 016806 (2013).
- [41] B. Carvalho, Y. Wang, S. Mignuzzi, D. Roy, M. Terrones, C. Fantini, V. H. Crespi, L. M. Malard, and M. A. Pimenta, Intervalley scattering by acoustic phonons in two-dimensional MoS₂ revealed by double-resonance Raman spectroscopy, *Nat. Commun.* **8**, 14670 (2017).
- [42] B. Zhu, H. Zeng, J. Dai, Z. Gong, and X. Cui, Anomalously robust valley polarization and valley coherence in bilayer WS₂, *Proc. Natl. Acad. Sci. U.S.A.* **111**, 11606 (2014).
- [43] P. K. Nayak, F.-C. Lin, C.-H. Yeh, J.-S. Huang, and P.-W. Chiu, Robust room temperature valley polarization in monolayer and bilayer WS₂, *Nanoscale* **8**, 6035 (2016).
- [44] H. Sigurdsson, A. J. Ramsay, H. Ohadi, Y. G. Rubo, T. C. H. Liew, J. J. Baumberg, and I. A. Shelykh, Driven-dissipative spin chain model based on exciton-polariton condensates, *Phys. Rev. B* **96**, 155403 (2017).